International Journal of Pharmaceutics 666 (2024) 124833

Contents lists available at ScienceDirect

International Journal of Pharmaceutics

journal homepage: www.elsevier.com/locate/ijpharm

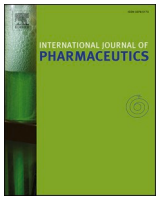

Assessing processability of milled HME extrudates: Consolidating the effect of extrusion temperature, drug loading, and particle size via Non-dimensional cohesion

Christopher Kossor, Roopal Bhat, Rajesh N. Davé *

New Jersey Center for Engineered Particulates, New Jersey Institute of Technology, Newark, NJ 07102, USA

ARTICLE INFO

Keywords:
Hot melt extrusion
Amorphous solid dispersion
Flowability
Cohesion
Bond number

ABSTRACT

The downstream processability of Hot Melt Extrusion (HME) Amorphous Solid Dispersions (ASD), an underexplored topic of importance, was assessed through a multi-faceted particle engineering approach. Extrudates, comprised of griseofulvin (GF), a model poorly water-soluble drug, and hydroxypropyl cellulose (HPC), were prepared at four drug concentrations and three HME temperature profiles to yield cases with and without residual crystallinity and subsequently milled to five sieve cuts ranging from < 45 μm to 355 – 500 μm. Solid state characterization was performed with XRPD, FT-IR, and TGA. Particle scale properties of the milled extrudates were evaluated including particle size, density, surface energy, and morphologies imaged via SEM. It was observed that regardless of sieve cut size, drug concentration and HME conditions impacted the flowability trends, quantified via Flow Function Coefficient (FFC) and bulk density. As a novelty, the effects of various process parameters and drug loadings were consolidated into a dimensionless interparticle cohesion measure, granular Bond Number (Bo_g), to better correlate them with bulk powder properties. The significant contrast in particle morphologies, particle size, and densities among selected cases demonstrated that particle size alone should not be the sole consideration when correlating particle scale to bulk powder scale properties of milled extrudates. Instead, the HME temperature profile and ASD drug loading may be more suitable parameters affecting the bulk powder properties of the milled extrudates.

1. Introduction

The limited bioavailability of nearly 75 % of Active Pharmaceutical Ingredients (API) under development and 90 % of new chemical entities is a fundamental concern stemming from inadequate solubility and permeability once ingested (Benet et al. 2011, Iyer et al. 2021). The inability of these low bioavailability APIs to achieve and maintain aqueous supersaturation solubility is due to the highly ordered structure and low thermodynamic free energy of the crystalline form (Brouwers et al. 2009, Newman et al. 2012). In principle, the amorphous form of the API can utilize the increased disorder and greater thermodynamic free energy to achieve aqueous supersaturation solubility much greater than the crystalline form. In practice, however, the amorphous API must be paired with an optimal matrix inducing polymer to form a molecularly dispersed single amorphous phase that resists crystal nucleation and growth, referred to as an Amorphous Solid Dispersion (ASD) (Sekiguchi et al. 1964, Chiou and Riegelman 1971, Hancock and Zografi 1997, Khougaz and Clas 2000, Marsac et al. 2006, Rumondor et al. 2009a, Mooter, 2011, Baghel et al. 2016, Moseson et al. 2020).

Hot Melt Extrusion (HME) is a favorable ASD manufacturing technique since it is a continuous, single step, and solventless process that is scalable (Breitenbach 2002, Mooter, 2011, Chivate et al. 2021). In particular, the API and polymer are blended, conveyed, heated, extruded, and quenched to form the extrudates. The key processing parameters to be tuned are the screw configurations, temperature profile, feed rate, screw speed, and quench rate, which all have been reported to impact the ability to form an ASD. However, the API and polymer must be selected to have high miscibility, preferably low API melting temperature, low viscosity, and are not thermally degraded during HME (Sarode et al. 2013, Mendonsa et al. 2020). The extrudates are quenched and subsequently milled (i.e., ball milling, cryo-milling, etc.) until the desired particle size distribution is obtained. A potential underexplored advantage of HME is that the milling processing stage can tune the particle size distribution to achieve favorable downstream

* Corresponding author.
E-mail address: dave@njit.edu (R.N. Davé).

https://doi.org/10.1016/j.ijpharm.2024.124833
Received 8 August 2024; Received in revised form 9 October 2024; Accepted 11 October 2024
Available online 15 October 2024

processing qualities, such as flowability, density, compaction, and dissolution. In general, large particles exhibit low particle cohesion and high flowability but experience insufficient tablet strength and dissolution rates. In contrast, fine particles exhibit high particle cohesion, poor flowability, and the possibility for inducing faster recrystallization due to larger surface area but offer proficient tablet strength and increased dissolution rates (Liversidge and Cundy 1995, Zheng et al. 2019).

Several studies have aimed to study ASD manufacturing techniques and their impact on bulk powder properties, e.g., flowability, bulk density, compaction, dissolution, etc., yet lacked the investigation of critical factors such as HME processing parameters, drug loading, milled extrudate particle size, and tablet compaction (Iyer et al. 2013, Davis et al. 2018, Huang and Williams 2018, Ekdahl et al. 2019, Schonfeld et al. 2021). Davis et al. (Davis et al. 2018) investigated the bulk powder properties and dissolution of a ternary ASD formulation consisting of Itraconazole, Soluplus®, and Hypromellose phthalate at a fixed concentration formed by two different techniques, spray drying and HME. The authors identified that the small particle size and morphology of the spray dried ASD yielded poor density and flowability while increased tabletability and dissolution compared to the larger, denser milled ASD extrudates. However, the milled ASD extrudate material was only produced at fixed HME conditions and the study only evaluated two broad sieve cuts, < 90 μm and $90 - 450$ μm. In particular, the bulk powder properties were evaluated based on the larger sieve cut leading to sub optimal bulk properties, compaction, and dissolution behavior, such as yielding Flow Function Coefficient (FFC) values beyond the usable range of 10 with high deviations. Lastly, the study used relatively larger-sized excipients, Avicel pH 200 LM and Mannogem, presumably as an attempt to enhance powder flow. Unfortunately, this created additional issues, such as decreased overall drug dosage and potential for segregation during the mixing of the milled ASDs and excipients. To date, none of these studies has investigated whether formulation and HME processing parameters can impact the particle scale properties and can have subsequent influence on bulk powder properties. Consequently, there is a technical gap regarding the preferred milled ASD particle size required to obtain particles that are not highly cohesive for processing purposes, form strong tablets, and obtain sustainable supersaturation conditions upon dissolution.

Therefore, developing an understanding of powder behavior by assessing particle scale properties, e.g., particle size distributions, particle surface energy, density, morphology, roughness, etc., is necessary to understand their influence on subsequent bulk powder and downstream processabilities such as flowability, content uniformity, compaction, and dissolution. Unfortunately, these topics have not been systematically investigated with milled ASD materials due to the challenging performance of fine pharmaceutical powders for downstream processing (Prescott and Garcia 2001, Hancock et al. 2002, Sinka et al. 2004, Nokhodchi et al. 2007, Xie and Puri 2007). Fundamentally, fine powders, typically 100 μm or smaller, are cohesive and their cohesion is the root cause behind these processability challenges since it leads to their poor flowability, low bulk density, agglomeration, etc., which adversely impacts the product quality and performance. Ideally, a mechanistic approach to estimate powder cohesion that accounts for particle size and other particle scale properties is necessary to understand the impact of ASD processing factors such as drug concentration and HME temperature on bulk powder properties.

An effective approach to model powder cohesion is a dimensionless parameter called granular Bond Number (Bo_g), which is the ratio of cohesive forces to body forces. In particular, if the powders are dry and uncharged, then the Bond number can be computed by the ratio of interparticle van der Waals force to particle weight (Nase et al. 2001, Yu et al. 2003, Castellanos 2005, Chen et al. 2008, Jallo et al. 2012a, Capece et al. 2014, Boonkanokwong et al. 2021, Kunnath et al. 2023). The nondimensionalized approach to model powder cohesion enables the consolidation of numerous factors, e.g., material properties, particle size, morphology, surface energies, surface roughness, etc., to counter the lack of mechanistically based predictions. Bond number provides relative guidance as to powder processibility; for example, when $Bo_g \leq 1$, particles are free flowing particles since gravity dominates. At the other extreme, when $Bo_g \gg 1$, particles are poorly flowing and interparticle force dominates. Therefore, estimating the granular Bond number will enable the capture of various ASD compositions and HME temperature profiles reflected in the particle scale properties of subsequently milled extrudates.

Thus, the primary purpose of this investigation is to attempt to consolidate the impact of drug loading, milled particle size, and HME temperature profile on particle scale and bulk powder properties of milled exudates into a nondimensional measure of cohesion referred to as granular Bond number, Bo_g. A high melting point, Biopharmaceutics Classification System class II drug, griseofulvin, was selected as a model drug to form an ASD with Hydroxypropyl Cellulose SL (HPC) as the matrix forming polymer. HME-formed extrudates at three temperature profiles were aimed at creating cases with and without residual crystallinity to provide a wider range of Bo_g analysis. The milled extrudates were sieved into five distinct sieve cut ranges from < 45 μm to 500 μm to provide narrow particle size distributions for a detailed investigation. Particle scale and bulk powder properties were measured for different drug loadings, processing temperatures, and particle size ranges. The particle size distribution, particle densities, surface energy, and surface roughness were assessed and a dimensionless measure of cohesion, Granular Bond number, was modeled to capture the impact of HME processing temperature, drug loading, and particle size.

2. Materials and methods

2.1. Materials

The Biopharmaceutics Classification System (BCS) class II drug, griseofulvin (GF; Hegno Shanghai, China), was selected as the model drug due to its tendency to crystallize rapidly (Baird et al. 2010), posing a challenge for effective ASD production with a glass transition temperature (T_g) of 90 °C and a melting point (T_m) of 220 °C (Rahman et al. 2020). Hydroxypropyl cellulose (HPC SL grade; Nisso America Inc., New York, NY, USA), a semi-crystalline polymer with the T_g of 86.2 °C (Luebbert et al., 2021) and T_m of around 170–200 °C was used as the model polymer (Rahman et al. 2020).

2.2. Methods

2.2.1. Preparation of extrudates

The HME temperature profiles and compositions of the powder blends for extrudate production are summarized in Table 1 and Table 2, respectively. The blends were mixed prior to HME feeding by a high-intensity vibrational mixer (LabRAM, Resodyn Acoustic Mixers, Inc., Butte, MT, USA) at a frequency of 60 Hz with an acceleration of 75 G for 5 min, as previously established (Buyukgoz et al. 2021). HME processing employed a 11 mm diameter co-rotating twin-screw extruder (Thermo Fisher Scientific Inc., Waltham, MA, USA) with a custom fabricated die with a diameter of 2 mm and a length of 38 mm. For all HME trials, the screw speed was 60 rpm, the powder feed rate was set to 2.4 g/min, and the screw configuration was set based on previous work (Buyukgoz et al. 2021). The different ranges of HME processing temperatures were selected to prepare extrudates with varying residual crystalline/

Table 1
Hot Melt Extrusion temperature profiles.

Profile	Die	Zone 8	Zone 7	Zone 6	Zone 5	Zone 4	Zone 3
170 °C	170	170	150	150	130	130	100
190 °C	190	190	170	170	150	150	100
210 °C	210	210	190	190	170	170	100

Table 2
Average PSD and standard deviations for all three HME temperatures for each of the five sieve cuts and four drug loadings.

GF (% w/w)	HPC – SL (w/w%)	Sieve Cut (μm)	d_{10} (μm)	d_{50} (μm)	d_{90} (μm)	$d_{3,2}$ (μm)
0	100	<45	4.59 ± 0.37	19.34 ± 1.09	48.86 ± 2.92	10.62 ± 0.58
		45 – 75	8.78 ± 0.76	46.94 ± 5.07	97.34 ± 4.26	19.28 ± 1.51
		75 – 125	54.18 ± 11.38	111.29 ± 8.31	184.78 ± 15.21	56.3 ± 10.56
		125 – 355	144.17 ± 48.5	263.31 ± 64.96	447.75 ± 70.76	196.68 ± 93.2
		355 – 500	298.51 ± 14.95	499.14 ± 5.83	770.45 ± 28.7	361.9 ± 55.36
10	90	<45	6.59 ± 1.06	23.07 ± 1.64	45.38 ± 1	13.26 ± 1.36
		45 – 75	23.97 ± 10.7	55.76 ± 7.79	89.37 ± 4.56	35.58 ± 10.89
		75 – 125	52.26 ± 12.77	99.89 ± 7.45	149.77 ± 3.38	68.65 ± 17.7
		125 – 355	123.79 ± 16.8	219.46 ± 17.01	387.92 ± 49.92	181.43 ± 23.69
		355 – 500	313.07 ± 7.47	490.16 ± 11.27	733.06 ± 56.51	399.87 ± 56.17
20	80	<45	7 ± 1.58	23.41 ± 2.69	44.91 ± 1.68	13.66 ± 2.04
		45 – 75	27.2 ± 9.23	58.35 ± 2.58	89.84 ± 0.73	38.55 ± 8.26
		75 – 125	63.62 ± 6.79	106.5 ± 1.97	156.47 ± 6.68	74.57 ± 15.95
		125 – 355	142.45 ± 3.01	241.82 ± 5.57	401.21 ± 19.15	209.88 ± 10.74
		355 – 500	312.52 ± 3.72	482.18 ± 13.09	717.45 ± 71.16	391.58 ± 60.56
30	70	<45	5.01 ± 1.06	21.43 ± 3.16	43.24 ± 1.28	11.37 ± 1.65
		45 – 75	24.01 ± 12.08	56.34 ± 5.19	88.4 ± 0.94	33.58 ± 11.31
		75 – 125	58.96 ± 7.93	101.9 ± 2.23	149.35 ± 2.52	57.7 ± 11.88
		125 – 355	130.88 ± 9.66	226.96 ± 26.13	382.1 ± 46.87	137.66 ± 47.55
		355 – 500	319.99 ± 10.6	483.33 ± 29.02	718.57 ± 95.09	383.96 ± 73.44

amorphous content.

2.2.2. Bulk extrudate milling via LabRAM

Extrudates were first milled with a high-intensity vibrational mixer (LabRAM, Resodyn Acoustic Mixers, Inc., Butte, MT, USA) for 5 min with an acceleration of 75 G at 60 Hz with 5 stainless steel ball bearings to break the large extrudates into particles < 500 μm for subsequent micronization.

2.2.3. Micronization of extrudates via Fluidized energy mill (FEM)

Further particle size reduction to obtain fine particles less than 125 μm was performed using a FEM (Pharmaceutical Micronizer Fluidized Energy Grinding Jet mill, Sturtevant Inc., Hanover, Massachusetts). The FEM process parameters such as feed rate, feed pressure, and grind pressure were fixed at 1 g/min, 75 psi, and 70 psi, respectively, based upon adapting process conditions from previous work to the milled extrudates of the current work (Han et al. 2013b, Chen et al. 2018a, Chen et al. 2020, Lin et al. 2024). A series of sieves (Dual Manufacturing Co., Inc., Franklin Park, Illinois, USA) were used to produce different particle size distributions using the following mesh sizes 45, 75, 125, 355, and 500 μm. The sieve cuts are summarized in the third column of Table 2.

2.2.4. Solid state characterization

The as-received GF, HPC, Physical Mixtures (PM), and milled extrudates were examined for X-Ray Powder Diffraction (XRPD) via Empyrean Series 2 X-ray Diffraction system (PANalytical, Westborough, MA, USA) to measure the extent of crystalline state of GF after thermal processing in HME and both milling operations. The samples were scanned at a 2θ angle ranging from 5° to 35° (0.01° step) with a Cu Kα radiation source operated at 45 kV and 40 mA. The divergence slit of the incident beam and anti-scatter slit were set to 1/4° and 1/2°, respectively, with a mask of 15 mm. The anti-scatter slit of the diffractive beam was set to 1/4°.

2.2.5. Fourier Transform infrared (FT-IR) Spectroscopy

The FT-IR spectra of 30 % GF 70 % HPC PM and milled extrudates processed at 170 and 210 °C were captured to assess the extent of drug – polymer interactions. An attenuated total reflectance (ATR) infrared spectrum was measured with 32 scans with a resolution of 4 cm^{-1} by an Agilent Cary 620 FT-IR (Santa Clara, CA, USA) equipped with single bounce diamond crystal and Golden Gate type ATR unit. The spectra were reported in the ranges of 1550 – 1750 cm^{-1} and 2800 – 3000 cm^{-1} wavenumbers.

2.2.6. Thermal stability

Potential thermal degradation was determined with thermogravimetric analysis (TGA) using a Perkin Elmer 8000 TGA (Perkin Elmer, Waltham, MA, USA). The 30 % GF 70 % HPC PM and milled extrudates processed at 170 and 210 °C were measured. Samples consisting of 3 – 5 mg were loaded into a crucible, heated from 30 to 300 °C at a rate of 10 °C/min, and cooled to 30 °C with a 60 ml/min flow of nitrogen.

2.2.7. Particle sizing

Particle size distribution statistics including D_{10}, D_{50}, D_{90}, and $D_{3,2}$ of all milled extrudates before and after FEM processing were measured by Sympatec Helos/Rodos volume-based laser diffraction particle size analyzer (Sympatec Inc., NJ). The Rodos dispersion was performed at 1 bar based on pressure titration and further details may be found in other papers (Huang et al. 2017, Kunnath et al. 2018, Kim et al. 2022, Kim et al. 2023). Two replicates were performed per powder. The particle size distributions were calculated by the Sympatec Windox 5.0 software and were summarized in Table 2.

2.2.8. Particle true density

The particle true density of each powder was measured by a helium multipycnometer (P/N 02029–1, Quantachrome Instruments, USA). The true density for each powder was the average of ten repeated measurements, reported in Table 3.

2.2.9. Particle morphology analysis: Scanning electron microscopy (SEM)

The morphology and roughness of < 45 μm size sieve cut of four select cases: 100 % HPC-SL 170 °C, 100 % HPC-SL 210 °C, 30 % GF 70 % HPC-SL 170 °C, and 30 % GF 70 % HPC-SL 210 °C were qualitatively characterized via a scanning electron microscopy (JSM-7900F, JEOL Ltd., Peabody, MA, USA). The samples were placed on an aluminum stub with carbon tape and sputter coated with gold (Q150T 16017, Quorum Technologies Ltd., Laughton, East Sussex, England). The particle aspect ratio was assessed by manually measuring the lengths and widths of a particle in triplicate and then taking the ratio of length to width, where length is the greater magnitude.

2.2.10. Particle surface energy measurements

The particle surface energy is a particle scale property required to calculate the interparticle force necessary for dimensionless assessment of cohesion analysis via granular Bond Number. The total particle surface energy of select cases of 75 – 125 μm size sieve cut milled extrudates: 100 % HPC-SL 170 °C, 100 % HPC-SL 210 °C, 30 % GF 70 % HPC-

Table 3
Particle scale properties used for Bond Number, Bo_g, calculations: Median Particle Size (D_{50}), Sauter Mean Diameter ($D_{3,2}$), Particle True Density (ρ), Dispersive Surface Energy (γ_d), and the last column presents the computed values for the Bond Number (Bo_g).

GF (w/w%)	HME T (°C)	Sieve Cut (μm)	D_{50} (μm)	$D_{3,2}$ (μm)	ρ (kg/m^3)	γ_d (mJ/m^2)	d_{asp} (nm)	Bo_g (−)
0	170	<45	19.65 ± 0.39	10.75 ± 0.22	1341	40.08	0	26941.20
		45–75	45.51 ± 1.07	18.47 ± 0.19	1283	40.08	0	9535.26
		75–125	116.38 ± 0.64	57.89 ± 0.39	1277	40.08	0	974.84
	210	<45	18.03 ± 0.16	9.94 ± 0.14	1341	39.39	0	30939.60
		45–75	42.15 ± 0.1	18.16 ± 0.05	1283	39.39	0	9693.86
		75–125	100.59 ± 0.36	43.80 ± 0.03	1277	39.39	0	1673.31
30	170	<45	17.355 ± 0.29	9.25 ± 0.11	1330	38.045	200	2260.55
		45–75	49.90 ± 0.77	20.66 ± 0.45	1345	38.045	200	200.44
		75–125	99.40 ± 1.42	44.72 ± 1.19	1317	38.045	200	20.17
	210	<45	23.57 ± 0.28	12.55 ± 0.05	1330	39.78	100	473.07
		45–75	61.09 ± 0.42	45.90 ± 1.07	1345	39.78	100	9.77
		75–125	102.15 ± 0.3	71.23 ± 0.6	1317	39.78	100	2.61

SL 170 °C, and 30 % GF 70 % HPC-SL 210 °C were analyzed. The total surface energy, the sum of the Liftshitz-van der Waals dispersive surface energy and the polarity component, was determined using automated inverse gas chromatography (SEA-IGC; Surface Energy Measurement Systems Ltd., UK). The details of sample preparation and analysis methods may be found elsewhere (Han et al. 2013a, Han et al. 2013b). The reported total dispersive surface energy for each powder was the average of two repeated measurements, reported in Table 3.

2.2.11. Bulk flow and density assessments

The bulk powder density and bulk powder flowability were assessed with a FT4 powder rheometer (FT4, Freeman Technology, UK). The bulk powder density and bulk powder flowability were measured with an acrylic cylinder of 25 mL × 25 mm and 10 mL × 25 mm, respectively. A pre-shear normal stress of 3 kPa was utilized for all measurements. The Flow Function Coefficient, (FFC), was used to quantify the bulk powder flowability and is determined by the ratio of the major principal stress and unconfined yield strength (Freeman 2007). There are five flow regimes that the FFC outcomes can be classified into: *no flow* ($0 < FFC < 1$), *very cohesive* ($1 < FFC < 2$), *cohesive* ($2 < FFC < 4$), *easy-flow* ($4 < FFC < 10$), and *free-flow* ($10 < FFC$) (Schulze 2008, Schulze 2021). Details of the FT4 testing may be found elsewhere (Huang et al. 2017, Kim et al. 2021). Bulk density and flowability measurements were repeated in triplicate.

3. Results and discussion

3.1. Fabrication of milled ASDs

3.1.1. Crystallinity

The milled extrudates for all formulations and HME temperatures were characterized by XRPD immediately after each of the two milling steps to determine any solid-state changes to GF. The diffractograms are summarized in Fig. 1. The Physical Mixtures (PM) represent the as-received materials where the characteristic peaks of GF indicated the presence of crystallinity while the HPC halo patterns indicated it to be amorphous or a non-detectable amount of crystallinity. The extrudates with the lowest GF concentration, 10 %, resulted in the absence of characteristic GF peaks and the presence of halo patterns at all HME operating temperatures (Fig. 1a), suggesting that all HME temperatures at this low level of drug loading produce an ASD due to the API – polymer miscibility. Next, ASDs were obtained for the 20 % GF mixture only when the HME temperature was above 190 °C since the characteristic GF peaks were present in the 170 °C curve and absent in the 190 °C and 210 °C curves, leaving only halo patterns (Fig. 1b). Lastly, the 30 % GF mixture only resulted in an ASD during HME with the highest operating temperature, 210 °C, since this is only curve without characteristic GF peaks (Fig. 1c). The presence of the halo patterns is indicative of successfully obtaining ASDs not only after HME, but also after both milling steps. Lastly, these solid state XRPD results align with previous work that investigated a similar GF – HPC composition and range of HME (Gorkem Buyukgoz et al. 2020, Buyukgoz et al. 2021). It must be noted that the approximately 5 % crystallinity detection limit of

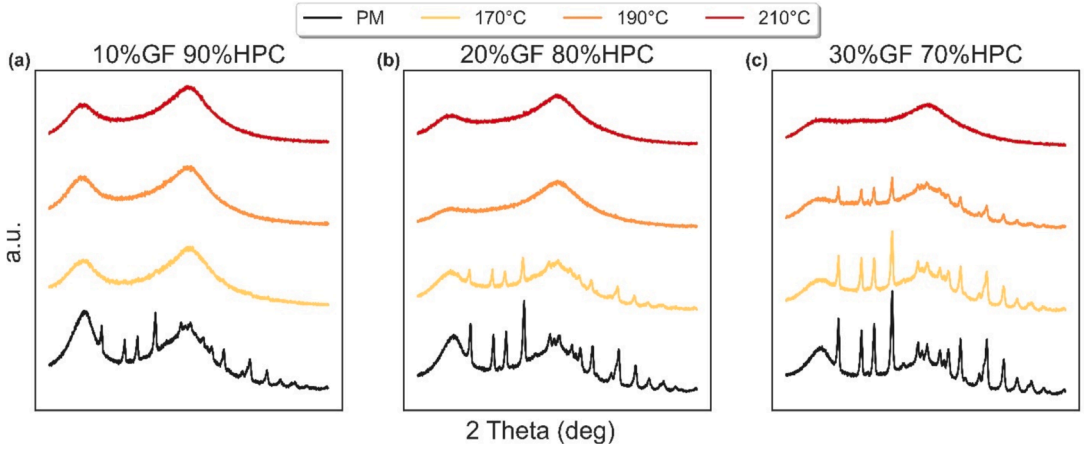

Fig. 1. XRPD diffractograms of the GF/HPCSL physical mixtures and milled HME extrudates for three temperature profiles for three drug loadings: a) 10% GF, b) 20% GF, and c) 30% GF.

XRPD may leave residual crystallinity undetected despite the cases with an absence of GF characteristic peaks (Venkatesh et al. 2001, Dedroog et al. 2020). Further processing adjustments, such as increased extrusion temperature, residence time distribution, and quench rate may need to be investigated in a future study to decrease the probability of residual crystallinity and or amorphous phase separation (Lu et al. 2016).

3.1.2. FT-IR Spectroscopy

The FT-IR spectra of 30 % GF 70 % HPC PM and milled extrudates processed at 170 and 210 °C are presented in Fig. 2 to further assess the drug and polymer molecular interactions. The FT-IR spectrum of the PM exhibited GF characteristic peaks in the 1550 – 1800 cm^{-1} region, which indicates the C = O stretching vibrational frequencies (Bennett et al. 2015). Moreover, the IR spectra can demonstrate the presence of hydrogen bonding resulting from the strong drug and polymer molecular interactions in an ASD by observing changes to peak shapes (Rumondor et al. 2009b, Rahman et al. 2020). The peak intensities diminished as HME temperature increased from 170 °C, residual crystallinity, to 210 °C, amorphous. It was expected that hydrogen bonds were present between the carbonyl groups of GF and the hydroxyl groups of HPC (Sarode et al. 2014). For instance, the peak at 1598 cm^{-1} diminished at both HME temperatures and both neighboring peaks broadened and shifted. In addition, the peak at 1658 cm^{-1} broadened and split into two sub-peaks for the 170 °C case and a shifted, diminished peak for the 210 °C case, representing both free and bound C = O stretchings resulting from the hydrogen bond interactions with the hydroxyl groups of polymer HPC. Previous studies have also shown similar behavior of GF with polymers in ASDs (Al-Obaidi and Buckton 2009). These inferences to the degree of hydrogen bonding indicated a greater degree of amorphization of the milled extrudates processed at 210 °C compared to the 170 °C case, supporting the observations from the XRPD.

3.1.3. Thermal stability

The results for the thermo-gravimetric analysis (TGA) are presented in Fig. 3. The weight loss for all the tested samples was less than 1 % at 100 °C, which could be attributed to free or bound water (Tidau et al. 2019). The PM and two drug loadings, placebo and 30 % GF, extruded at the highest temperature, 210 °C, maintained less than 4 % weight loss at 250 °C. Thus, a maximum HME processing temperature of 210 °C was not expected to cause any degradation. Therefore, no thermal degradation was observed for the placebo and 30 % GF drug loadings at all HME processing temperature studied.

3.2. Particle properties of milled ASDs

3.2.1. Particle sizing

All twelve cases, three HME profiles and four drug loadings, were each milled and sieved into the five sieve cuts, which was necessary for the multi-faceted particle and bulk powder characterization. Each sieve cut particle size distribution reported is an average of 12 particle size distributions from three HME temperatures per four drug loadings and are provided in Fig. 4 while a summary of the particle size distribution statistics D_{10}, D_{50}, D_{90}, and $D_{3,2}$, are represented in Table 2. The narrow distributions are necessary to study the particle size impact on bulk properties such as flowability and bulk density.

3.2.2. Particle morphology – SEM

Particle morphology is a contributing factor to bulk powder properties. However, existing literature seldom investigates the impact of HME manufacturing parameters on particle morphology. Imaging techniques may be used to gather meaningful information using optical particle sizers, e.g., QicPic, Sympatec. Those instruments provide statistically meaningful yet highly averaged values for various morphological measures including particle shape or aspect ratios and may not provide sufficient detail of the particle surface roughness. In this study, SEM imaging was used instead, because it can provide qualitative insight on the particle morphology, such as shape and roughness, to observe any impact that drug loading and HME temperature can have on particle properties.

The milled extrudates were imaged via SEM and appeared as dense granules without a defined shape that had a varying degree of roughness and elongation depending on the drug loading and HME processing temperature, shown in Fig. 5. All SEM images were selected in the < 45 μm and 355 – 500 μm sieve cuts for two drug loadings and two HME temperatures. The placebo particles, Fig. 5e, f, g, and h, exhibited a greater aspect ratio than the 30 % GF particles, Fig. 5a, b, c, and d, which supported the aspect ratio results in Fig. 6. Furthermore, a striking difference in surface roughness can be seen in the GF loaded particles produced at 170°C and 210 °C. The 30 % GF case processed at 210 °C yielded particles with low surface roughness and clear fractures from milling. In contrast, the 30 % GF particles processed at 170 °C exhibited a very rough surface likely due to the incomplete melting of GF crystals and immiscibility from insufficient heat transfer. Thus, the difference in extrusion temperature profile impacted the surface roughness for a given drug loading by limiting the degree of crystallinity in the granule. Furthermore, the immiscibility of the GF and HPC at the low HME temperature, 170 °C, is in agreement with other similar SEM images

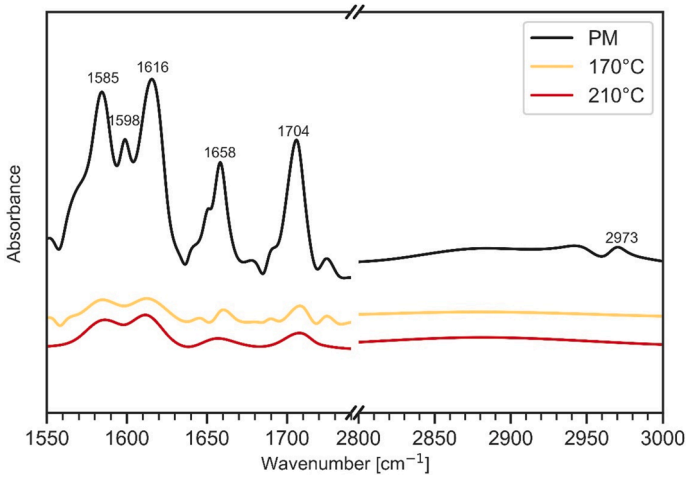

Fig. 2. FT-IR spectra of 30 % GF 70 % HPCSL physical mixture and milled extrudates for two HME temperatures, 170 °C and 210 °C.

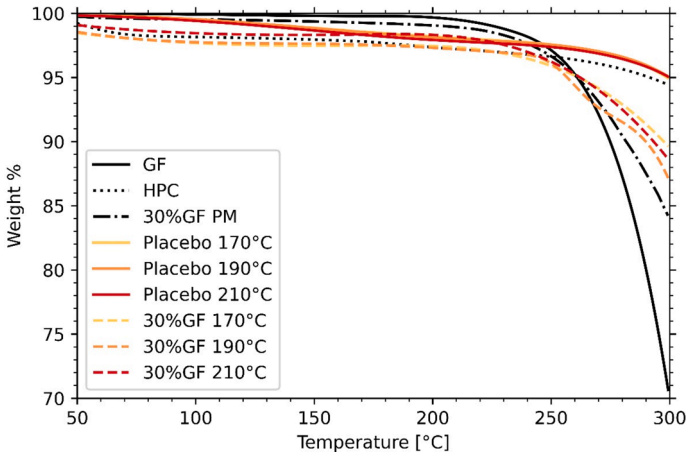

Fig. 3. TGA thermograms of GF, HPC, GF/HPC physical mixture, and milled extrudates for three HME temperatures and two drug loadings.

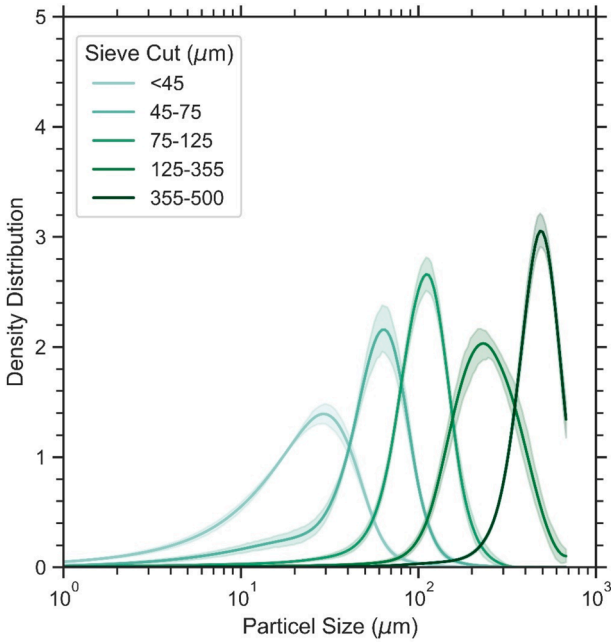

Fig. 4. Particle size distributions with shaded 95% confidence interval of each sieve cut consisting of three HME temperatures and four drug loadings per sieve cut.

(Buyukgoz et al. 2021). The range of surface roughness can be attributed to the different drug loadings and change in mechanical properties after extrusion at the two temperatures, thus varying milling dynamics could be encountered and influence extrudate breakage. In particular, the placebo particles extruded at the lower temperature profile exhibited more surface roughness than when extruded at a higher temperature profile; thus, the surface roughness is not only influenced by the presence of an API, but also the extrusion temperature. The increased surface roughness exhibited at the lower processing temperatures is a key factor, discussed in section 3.4, that contributes to particle interaction forces and ultimately to the behavior of bulk powder properties (Chen et al. 2008, Chen et al. 2009).

Additionally, particle morphological characteristics such as aspect ratio and elongation are commonly assessed to identify influence on subsequent bulk powder behavior (Gamble et al. 2015, Leane et al. 2015, Barjat et al. 2021, Gamble et al. 2023). In this study, drug loading had a significant contribution to the particle Aspect Ratio (AR), which is defined as length divided by width. The SEM images of all four drug loadings at two HME temperatures of the finest sieve cut were analyzed by repeatedly measuring the particle lengths and widths to calculate the AR and are illustrated in Fig. 5. The AR results are reported in Fig. 6, where the placebo cases have nearly double the AR compared to the API/polymer cases, which indicated that the placebo cases deviate more from spherical in shape. Most interestingly, AR for the 10 % GF, 20 % GF, and 30 % GF cases are comparable. It has been reported (Vrentas et al. 1988, Li et al. 2015, Flugel et al. 2021) that the mechanical properties of a glassy polymer with the presence of an API is strongly correlated to the degree of molecular mobility among the polymer and API, which can be characterized by the free volume of the system and molecular interactions. The different aspect ratios of the placebo and the GF loaded cases are likely due to differing breakage pathways among the neat polymer and the GF loaded cases. The change in mechanical properties, such as modulus and hardness, are likely due to the change in free volume and molecular interactions from the presence of the GF particles within the glassy polymer. Lastly, the HME temperature of the sample was found to have little influence on the measured aspect ratio.

3.3. *Bulk powder properties of milled ASDs*

There is significant interest (Demuth et al. 2015, Bhujbal et al. 2021, Monschke et al. 2021) in developing formulations that utilize ASD particles with large surface areas to promote desirable compression behavior while minimizing excessive excipient usage and rapid dissolution. However, finer particles, which have large surface area, typically suffer from low density and poor flowability due to excessive interparticle cohesion compared to their body forces (Davé et al. 2022, Kunnath et al. 2023). Hence, particle sizes well below normally reported in ASD HME literature, i.e., < 125 μm, were the focus of this study. There are several techniques to characterize the bulk flowability such as Carr index, Hausner ratio, orifice meter, and shear tests (Thalberg et al. 2004, Ghoroi et al. 2013). The flowability assessment for this work was based on the FT4 powder rheometer shear test to quantify the FFC, the ratio of the major principal stress and unconfined yield strength. The FFC was analyzed per five sieve cuts, four drug concentrations, and three HME temperature profiles, depicted in Fig. 7. As expected, the particle size is the major contributing factor to the observed FFC as seen by the 75 – 125 μm curve, which was two flow regimes greater than the < 45 μm curve for all GF cases. The drug loading was another important factor for the observed FFC trend. The placebo cases exhibited the lowest FFC flow regime of *very cohesive* for the < 45 μm and 45 – 75 μm sieve cuts and the largest sieve cut resulted in the cohesive flow regime. In contrast, the finest sieve cut for the 30 % drug load case yielded *easy-flow* regime despite its finer PSD and identical milling conditions. Interestingly, the FFC increases with increasing drug loading for the residual crystalline (170 °C) and ASD (210 °C) cases for all three sieve cuts. The observed

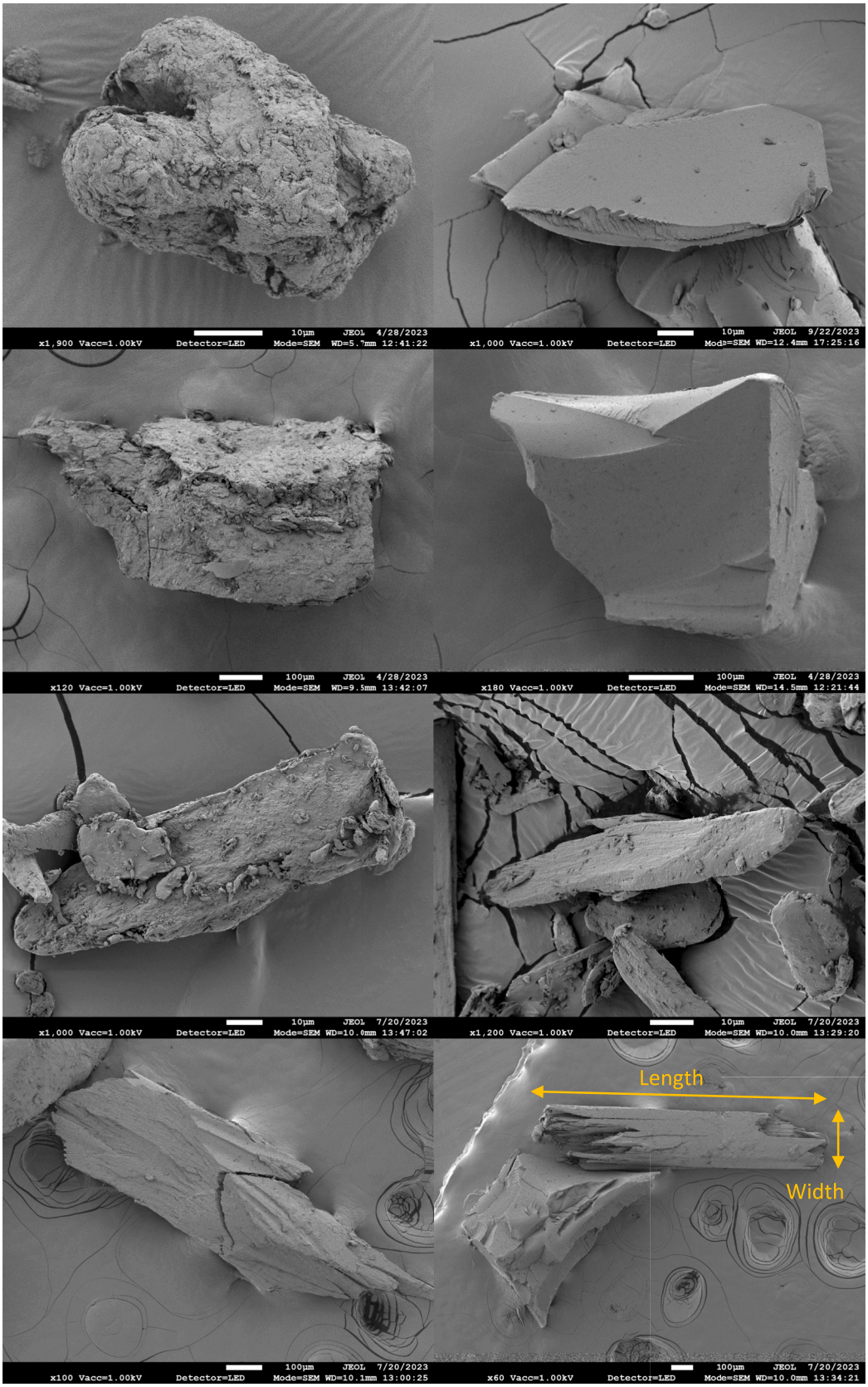

Fig. 5. SEM images of 30 % GF 70 % HPCSL and placebo milled extrudates of two sieve cuts and two HME temperature: a) 30 % GF 70 % HPCSL 170 °C < 45 µm, b) 30 % GF 70 % HPCSL 210 °C < 45 µm, c) 30 % GF 70 % HPCSL 170 °C 355 – 500 µm, d) 30 % GF 70 % HPCSL 210 °C 355 – 500 µm, e) 100 % HPCSL 170 °C < 45 µm, f). 100 % HPCSL 210 °C < 45 µm, g) 100 % HPCSL 170 °C 355 – 500 µm, h) 100 % HPCSL 210 °C 355 – 500 µm.

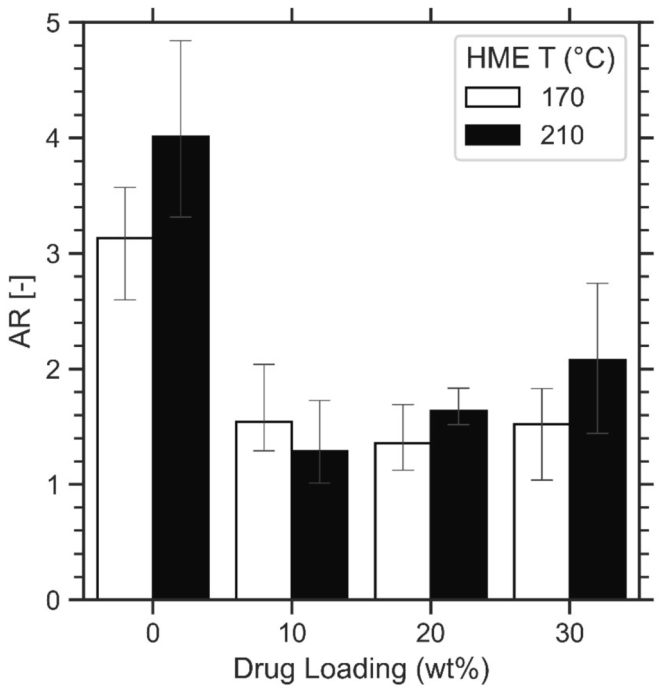

Fig. 6. Aspect ratio of exemplary GF/HPCSL milled HME extrudate powders of four drug loadings and two HME temperatures for the finest sieve cut, 170 °C and 210 °C.

trend between FFC and drug loading for a given sieve cut is likely due to the variation in particle scale properties for each drug loading such as surface roughness and density, which are both discussed in Section 3.4.

In addition to flowability, powder bulk density is another major indicator of the extent of powder cohesion (Abdullah and Geldart 1999). In fact, it has been compared to FFC in a phase map to better discern the bulk property enhancement trends, as it avoids the ubiquitous scatter found in individual particle scale measurements such as size distribution, morphology, surface roughness, and material properties (Mullarney et al. 2011, Kunnath et al. 2021). A plot of FFC and bulk density can reveal the trend of property enhancements due to major control variables such as the size, processing parameters, and formulation since a movement from the lower-left quadrant to upper-left quadrant indicates a more desirable state (Kunnath et al. 2021). Consequently, the FFC and conditioned bulk density are plotted in a phase map, Fig. 8, for the three finest sieve cuts, while the two largest sieve cuts were omitted, as they are categorized as belonging to the *free-flow* regime. The phase map is divided into quadrants such that the top right quadrant represents the properties necessary for direct compression downstream processing where a conditioned bulk density > 0.38 g/ml and FFC > 6.8 is desired (Shi et al. 2011, Chen et al. 2018b, Chen et al. 2019, Li et al. 2019, Lin et al. 2024). The drug loading had a noticeable impact on both FFC and bulk density, which was evident even at the finest particle size sieve cut (<45 μm) since 10 % GF had a FFC of 2.44 ± 0.05 to 2.7 ± 0.07 and 30 % GF had a FFC of 4.33 ± 0.23 to 5.2 ± 0.7 depending on the HME temperature. The HME temperature had a noticeable impact on bulk density, yet only had a subtle impact on flowability at each sieve cut and drug loading. For example, the 30 % GF case at the smallest sieve cut improved from 0.433 ± 0.012 g/ml to 0.485 ± 0.018 g/ml by increasing the HME temperature from 170 °C to 210 °C, respectively. These results indicated that the FT4 powder rheometer exhibited excellent sensitivity and low deviation for the FFC and bulk density measurements due to the careful consideration of measuring distinct sieve cuts, one of the novelties of this work. This approach improves upon methodologies with excessive scatter reported in other existing studies of the downstream processability of milled HME ASD material where sieve cuts were not considered (Davis et al. 2018). The results in this section established the effect of drug loading and HME temperature on bulk powder properties. However, a mechanistic understanding that consolidates multiple process parameters, drug concentration, and particle scale properties would be even more beneficial and was explored in the next section through a measure of nondimensional cohesion.

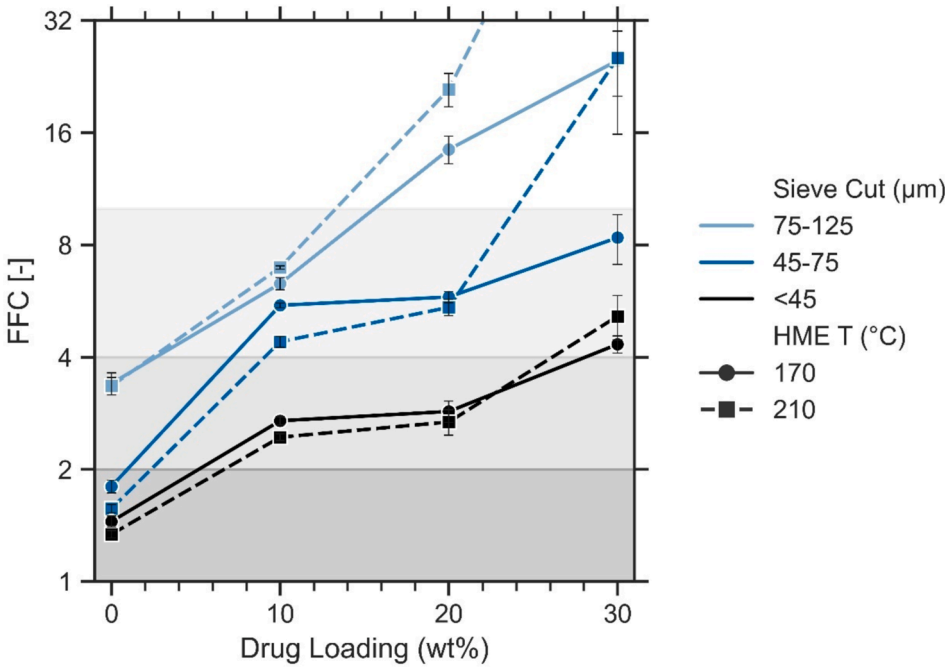

Fig. 7. Flowability Function Coefficient (FFC) of exemplary GF/HPC milled HME extrudate powders of four drug loadings, three sieve cuts, and two HME temperatures, 170 °C and 210 °C. The FFC axis is capped at 32 due to being much greater than the boundary for the free-flow regime of 10.

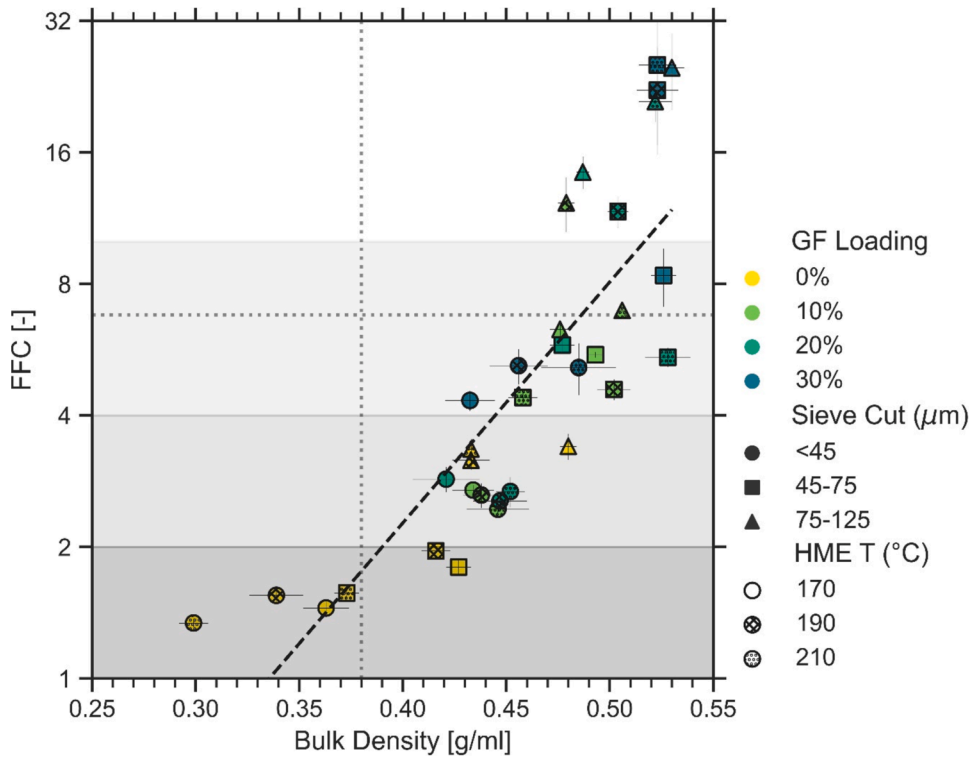

Fig. 8. Flowability Function Coefficient (FFC) and conditioned bulk density plot of exemplary GF/HPCSL milled HME extrudate powders. The varying colors represent four drug loadings of GF. The varying marker shapes represent three different sieve cut sizes. The varying hatch infill represents the three different HME processing temperatures. The shaded regions represent the four FFC regimes (bottom) very cohesive to (top) free flowing. The vertical dashed line represents bulk density criteria for direct compression (0.38 g/ml) and the horizontal dashed line represents the FFC criteria for direct compression (6.8).

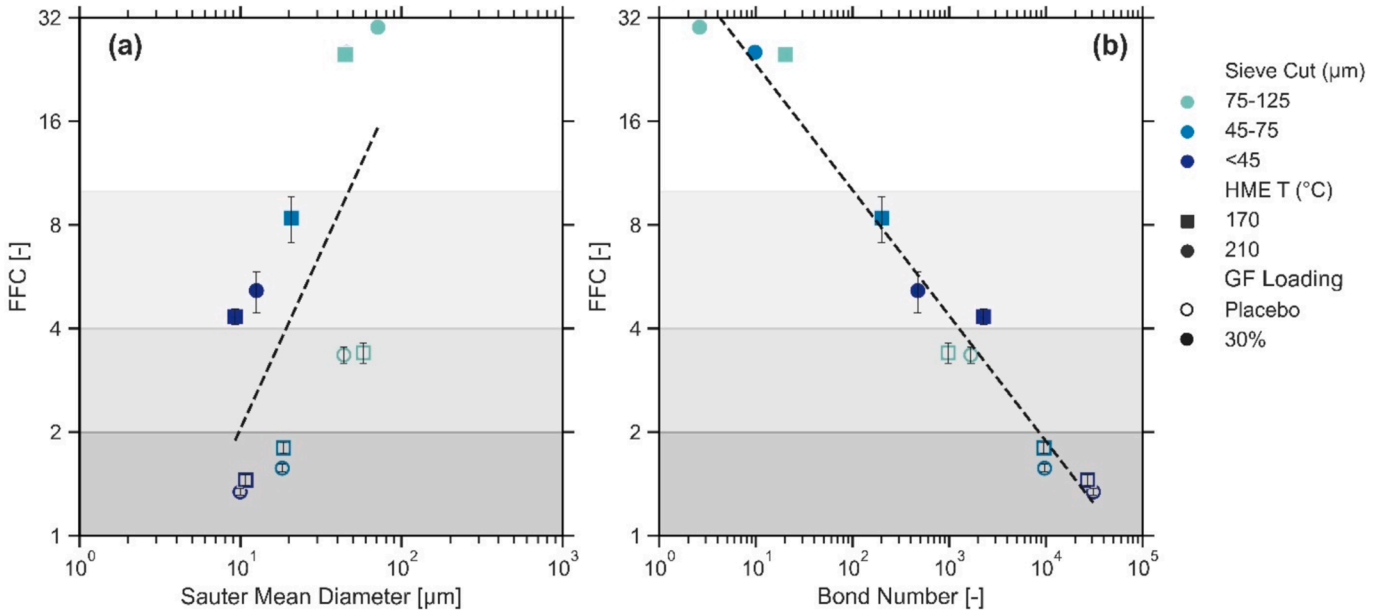

Fig. 9. Plots of a). FFC vs SMD and b). FFC vs Bog of 30 % GF 70 % HPCSL ASD and neat HPCSL polymer for the three finest sieve cuts and two HME temperatures, 170 °C and 210 °C. The shaded regions represent the four FFC flow regimes from (bottom) very cohesive to (top) free flowing.

3.4. Nondimensional particle cohesion: Granular bond number, Bo_g

The poor flowability behavior of the finer sieve cut particles was partially expected due to their inherently small median particle sizes, as demonstrated in Figs. 7 and 8. Upon initial inspection, the impact of particle size was readily seen where the smallest sieve cut has the smallest FFC and the largest size sieve cut has the greatest FFC for a given drug loading and HME temperature. However, comparing bulk powder properties such as FFC only to particle size fails to capture the impact from HME processing and drug loading, thus normalization of cohesive and gravitational forces is desired. Specifically, plotting FFC and Sauter mean diameter ($D_{3,2}$) particle size, as in Fig. 9a, leads to excessive scatter since the neat polymer and 30 % GF cases have similar particle size, yet drastically different FFC and flow regimes. Therefore,

such a plot failed to capture influences from other key particle scale measurements such as density, surface energy, and surface roughness.

Fundamentally speaking, the challenges faced in the processability of fine powders stem from their cohesive behavior, which is attributed to several factors, including, particle size distribution, morphology, density, surface energy, surface roughness, and environmental conditions (Gamble et al. 2011, Jallo et al. 2012b, Kunnath et al. 2021, Davé et al. 2022). Overall, although it depends on the combination of interparticle forces, cohesion for dry uncharged powders was dominated by van der Waals interactions, which was estimated by the Chen – NJCEP multi-asperity model (Chen et al. 2008). Accordingly, the interparticle cohesive force, F_{vdW}, which can be expressed by Eq. (1), was calculated for the milled extrudates by assuming the particles were monodispersed spherical particles with uniform monodispersed spherical asperities. The Hamaker constant is a function of dispersive surface energy at each contact as per Eq. (2).

$$F_{vdW} = \frac{Ad_{asp}}{8{z_0}^2} + \frac{AD}{24\left(2d_{asp} + z_0\right)^2} \tag{1}$$

$$A = 24\pi {D_0}^2 \gamma_d \tag{2}$$

In the above equations, d_{asp} is the asperity size, z_0 is the minimum separation distance between two particles, the typical value being 0.4 nm (Israelachvili, 1992, Johno et al. 2009), D is the particle size, usually the Sauter Mean diameter, A is the Hamaker constant calculated by Eq. (2), where D_0 is the minimum separation distance (assumed to be 0.165 nm) and γ_d is the dispersive surface energy measured by inverse gas chromatography (Han et al. 2013b, Jallo and Dave 2015, Kim et al. 2022). There are several methods proposed to select the asperity size, including an assumption of 200 nm for all powders (Massimilla and Donsì 1976), empirical functions of primary particle size (Yu et al. 2003), atomic force microscopy, and qualitative observation through SEM image analysis (Kim et al. 2022). All methods have varying degrees of uncertainty (Davé et al. 2022, Kunnath et al. 2023), but individual SEM estimations of powders of interest were the most attainable and relevant for this study.

Assessing the bulk powder properties behavior, e.g., flowability, bulk density, etc., solely based on median particle size is typically futile since the relationship between powder cohesion and particle size must be viewed by not only the linear relationship of size and cohesive forces, such as van der Waals (vdW), but also by the cubic relationship of size and relevant body forces, such as particle weight. Thus, the dimensionless measure of cohesion was applied to the particle scale properties to consolidate the effect of HME temperature profile, drug loading, and particle size. Bond number, Bo_g, is defined in Eq. (3).

$$Bo_g = \frac{F_{vdW}}{W_g} \tag{3}$$

As seen above, F_{vdW} is the interparticle cohesive force calculated by the Chen-NJCEP multi-asperity model in Eq. (1) and W_g is the particle weight. The particle weight can be calculated by Eq. (4) where D is the particle size, usually the Sauter Mean diameter, ρ is the particle true density, and g is the acceleration due to gravity and is approximated to be 9.8 m/s^2.

$$W_g = \frac{\pi}{6} D^3 \rho g \tag{4}$$

Bond Number (Bo_g) can be utilized as a scaling parameter to reflect differences in particle properties such as densities, surface energies, and roughness between largely crystalline and amorphous (ASD) materials. Moreover, Bo_g may capture the effect of drug loading and HME temperature on particle scale properties (size, roughness, density, and surface energy), thus enabling the prediction of bulk powder properties such as FFC. Table 3 summarizes the four key parameters for Bo_g calculation: Median Particle Size (D_{50}), Sauter Mean Diameter ($D_{3,2}$), Particle True Density (ρ), and Dispersive Surface Energy (γ_d). The surface roughness for the placebo cases was assumed to be smooth, while the 30 % GF cases were assumed to be 100 nm for the 210 °C case and 200 nm for the 170 °C cased, based upon SEM images in Fig. 5. These values were picked as rough estimates to capture the general effect of the characteristic roughness. The surface energies were measured for the placebo and 30 % GF cases both at 170°C and 210 °C and exhibited nearly the same values of approximately 40 J/m^2. The particle true densities were measured and ranged from 1277 to 1341 kg/m^3. The subsequent Bo_g values were calculated using Eqs 2 – 5 and plotted with FFC values in Fig. 9b.

Bond number analysis yielded significantly less scatter between FFC and Bo_g, Fig. 9b, compared to FFC versus SMD, Fig. 9a, since particle size distribution is not the only contributing factor affecting bulk properties. The estimated Bond Numbers are summarized in Table 3 for the selected drug loadings, HME temperatures, and sieve cuts. The 30 % GF loaded cases range from a Bo_g from 2.61 to 2260.55 and are classified by easy and free flowing regimes, respectively, while the placebo cases exhibit Bo_g ranging from 974 0.84 to 30939.60 and are classified by the cohesive and very cohesive flow regimes, respectively. Interestingly, the < 45 μm sieve cut of 30 % GF for 170 °C and 210 °C have similar FFC values, 4.33 ± 0.23 and 5.15 ± 0.7 and Bo_g values, 2260.55 and 473.07, respectively to the larger 75 – 125 μm sieve cut of placebo for 170 °C and 210 °C FFC values, 3.4 ± 0.23 and 3.35 ± 0.18 and Bo_g values, 974.84 and 1673.31. Moreover, the individual particle scale properties of those four contrasting cases can meaningfully be consolidated by a single nondimensionalized parameter, Bo_g, despite the drastically different particle sizes and morphologies between these two scenarios. Thus, Bo_g analysis can well capture the effects of drug load, particle size sieve cut, and HME temperature profiles. Future work may consider investigation to understand the impact of material selection, such as varying polymer type and molecular weight, and other HME key process parameters, such as screw configuration, quench rate, and milling conditions.

4. Conclusion

The impact of drug loading, HME operating conditions, and particle size on particle scale properties and bulk scale properties of milled HME extrudates was investigated with a multi-faceted approach. The constant milling conditions produced PSDs with similar statistics, indicating that final particle size measured by laser diffraction techniques was not heavily influenced by drug loading or HME operating temperature. The particle morphology was highly dependent on drug loading and HME operating temperature as the placebo cases yielded higher aspect ratio particles in contrast to the lower aspect ratio particles of the API and polymer combinations. The HME temperature determined whether residual crystallinity would be present or absent in the extrudates, which impacted the surface roughness of the particles. The ASD particles had significantly less roughness than their crystalline counterparts. These observations make a novel case in identifying how the key process parameter of HME temperature can influence downstream processing in terms of flowability and bulk density. Utilizing the granular Bond number appeared to be an effective approach to capture the impact of HME processing parameters and drug concentration on particle scale and bulk powder properties. Further investigation of the Bond number may help establish a viable approach to help with polymer selection and additional HME parameters for subsequent assessment of downstream processability.

CRediT authorship contribution statement

Christopher Kossor: Writing – review & editing, Writing – original draft, Visualization, Validation, Methodology, Investigation, Formal analysis, Data curation, Conceptualization. **Roopal Bhat:** Writing – review & editing, Investigation. **Rajesh N. Davé:** Supervision, Conceptualization, Formal analysis, Data curation, Writing – reorganization,

Writing – review & editing, Visualization, Resources, Funding acquisition.

Funding

Financial support from the National Science Foundation (NSF) grant IIP- 2,137,209 (NSF-IUCRC) along with the associated Industry Advisory Board (IAB) membership support to the Center for Materials Science and Engineering of Pharmaceutical Products (CIMSEPP), is gratefully acknowledged.

Declaration of competing interest

The authors declare that they have no known competing financial interests or personal relationships that could have appeared to influence the work reported in this paper.

Acknowledgements

The authors thank the CIMSEPP IAB mentors, especially Colleen Neu and Wuhong Yu, for their guidance. Generous donations of materials and characterization instruments are acknowledged from Nisso America Inc. and Surface Measurement Systems.

Data availability

Data will be made available on request.

References

Abdullah, E.C., Geldart, D., 1999. The use of bulk density measurements as flowability indicators. Powder Technol. 102 (2), 151–165.
Al-Obaidi, H., Buckton, G., 2009. Evaluation of griseofulvin binary and ternary solid dispersions with HPMCAS. AAPS PharmSciTech 10 (4), 1172–1177.
Baghel, S., Cathcart, H., O'Reilly, N.J., 2016. Polymeric Amorphous Solid Dispersions: A Review of Amorphization, Crystallization, Stabilization, Solid-State Characterization, and Aqueous Solubilization of Biopharmaceutical Classification System Class II Drugs. J. Pharm. Sci. 105 (9), 2527–2544.
Baird, J.A., Van Eerdenbrugh, B., Taylor, L.S., 2010. A classification system to assess the crystallization tendency of organic molecules from undercooled melts. J. Pharm. Sci. 99 (9), 3787–3806.
Barjat, H., Checkley, S., Chitu, T., Dawson, N., Farshchi, A., Ferreira, A., Gamble, J., Leane, M., Mitchell, A., Morris, C., Pitt, K., Storey, R., Tahir, F., Tobyn, M., 2021. Demonstration of the Feasibility of Predicting the Flow of Pharmaceutically Relevant Powders from Particle and Bulk Physical Properties. J. Pharm. Innov. 16 (1), 181–196.
Benet, L.Z., Broccatelli, F., Oprea, T.I., 2011. BDDCS applied to over 900 drugs. AAPS J. 13 (4), 519–547.
Bennett, R.C., Keen, J.M., Bi, Y.V., Porter, S., Durig, T., McGinity, J.W., 2015. Investigation of the interactions of enteric and hydrophilic polymers to enhance dissolution of griseofulvin following hot melt extrusion processing. J. Pharm. Pharmacol. 67 (7), 918–938.
Bhujbal, S.V., Mitra, B., Jain, U., Gong, Y., Agrawal, A., Karki, S., Taylor, L.S., Kumar, S., Tony Zhou, Q., 2021. Pharmaceutical amorphous solid dispersion: A review of manufacturing strategies. Acta Pharm. Sin. B 11 (8), 2505–2536.
Boonkanokwong, V., Khinast, J.G., Glasser, B.J., 2021. Scale-up and flow behavior of cohesive granular material in a four-bladed mixer: effect of system and particle size. Adv. Powder Technol. 32 (12), 4481–4495.
Breitenbach, J., 2002. Melt extrusion: from process to drug delivery technology. Eur. J. Pharm. Biopharm. 54 (2), 107–117.
Brouwers, J., Brewster, M.E., Augustijns, P., 2009. Supersaturating drug delivery systems: the answer to solubility-limited oral bioavailability? J. Pharm. Sci. 98 (8), 2549–2572.
Buyukgoz, G.G., Kossor, C.G., Davé, R.N., 2021. Enhanced Supersaturation via Fusion-Assisted Amorphization during FDM 3D Printing of Crystalline Poorly Soluble Drug Loaded Filaments. Pharmaceutics 13 (11).
Capece, M., Huang, Z., To, D., Aloia, M., Muchira, C., Davé, R.N., Yu, A.B., 2014. Prediction of porosity from particle scale interactions: Surface modification of fine cohesive powders. Powder Technol. 254, 103–113.
Castellanos, A., 2005. The relationship between attractive interparticle forces and bulk behaviour in dry and uncharged fine powders. Adv. Phys. 54 (4), 263–376.
Chen, H., Aburub, A., Sun, C.C., 2019. Direct Compression Tablet Containing 99% Active Ingredient-A Tale of Spherical Crystallization. J. Pharm. Sci. 108 (4), 1396–1400.
Chen, L., Ding, X., He, Z., Fan, S., Kunnath, K.T., Zheng, K., Dave, R.N., 2018a. Surface engineered excipients: II. Simultaneous milling and dry coating for preparation of fine-grade microcrystalline cellulose with enhanced properties. Int. J. Pharm. 546 (1–2), 125–136.
Chen, L., Ding, X., He, Z., Huang, Z., Kunnath, K.T., Zheng, K., Dave, R.N., 2018b. Surface engineered excipients: I. improved functional properties of fine grade microcrystalline cellulose. Int. J. Pharm. 536 (1), 127–137.
Chen, L., He, Z., Kunnath, K., Zheng, K., Kim, S., Dave, R.N., 2020. Fine grade engineered microcrystalline cellulose excipients for direct compaction: Assessing suitability of different dry coating processes. Eur. J. Pharm. Sci. 151, 105408.
Chen, Y., Yang, J., Dave, R.N., Pfeffer, R., 2008. Fluidization of coated group C powders. AIChE J 54 (1), 104–121.
Chen, Y., Quintanilla, M.A., Yang, J., Valverde, J.M., Dave, R.N., 2009. Pull-off force of coated fine powders under small consolidation. Phys. Rev. E Stat. Nonlin. Soft Matter Phys. 79 (4 Pt 1), 041305.
Chiou, W.L., Riegelman, S., 1971. Pharmaceutical applications of solid dispersion systems. J. Pharm. Sci. 60 (9), 1281–1302.
Chivate, A., Garkal, A., Dhas, N., Mehta, T., 2021. Hot-Melt Extrusion: An Emerging Technique for Solubility Enhancement of Poorly Water-Soluble Drugs. PDA J. Pharm. Sci. Technol. 75 (4), 357–373.
Davé, R., Kim, S., Kunnath, K., Tripathi, S., 2022. A concise treatise on model-based enhancements of cohesive powder properties via dry particle coating. Adv. Powder Technol. 33 (11).
Davis, M.T., Potter, C.B., Walker, G.M., 2018. Downstream processing of a ternary amorphous solid dispersion: The impacts of spray drying and hot melt extrusion on powder flow, compression and dissolution. Int. J. Pharm. 544 (1), 242–253.
Dedroog, S., Pas, T., Vergauwen, B., Huygens, C., Van den Mooter, G., 2020. Solid-state analysis of amorphous solid dispersions: Why DSC and XRPD may not be regarded as stand-alone techniques. J. Pharm. Biomed. Anal. 178, 112937.
Demuth, B., Nagy, Z.K., Balogh, A., Vigh, T., Marosi, G., Verreck, G., Van Assche, I., Brewster, M.E., 2015. Downstream processing of polymer-based amorphous solid dispersions to generate tablet formulations. Int. J. Pharm. 486 (1–2), 268–286.
Ekdahl, A., Mudie, D., Malewski, D., Amidon, G., Goodwin, A., 2019. Effect of Spray-Dried Particle Morphology on Mechanical and Flow Properties of Felodipine in PVP VA Amorphous Solid Dispersions. J. Pharm. Sci. 108 (11), 3657–3666.
Flugel, K., Schmidt, K., Mareczek, L., Gabe, M., Hennig, R., Thommes, M., 2021. Impact of incorporated drugs on material properties of amorphous solid dispersions. Eur. J. Pharm. Biopharm. 159, 88–98.
Freeman, R., 2007. Measuring the flow properties of consolidated, conditioned and aerated powders — A comparative study using a powder rheometer and a rotational shear cell. Powder Technol. 174 (1–2), 25–33.
Gamble, J.F., Chiu, W.S., Tobyn, M., 2011. Investigation into the impact of sub-populations of agglomerates on the particle size distribution and flow properties of conventional microcrystalline cellulose grades. Pharm. Dev. Technol. 16 (5), 542–548.
Gamble, J.F., Tobyn, M., Hamey, R., 2015. Application of image-based particle size and shape characterization systems in the development of small molecule pharmaceuticals. J. Pharm. Sci. 104 (5), 1563–1574.
Gamble, J.F., Akseli, I., Ferreira, A.P., Leane, M., Thomas, S., Tobyn, M., Wadams, R.C., 2023. Morphological distribution mapping: Utilisation of modelling to integrate particle size and shape distributions. Int. J. Pharm. 635, 122743.
Ghoroi, C., Gurumurthy, L., McDaniel, D.J., Jallo, L.J., Davé, R.N., 2013. Multi-faceted characterization of pharmaceutical powders to discern the influence of surface modification. Powder Technol. 236, 63–74.
Gorkem Buyukgoz, G., Soffer, D., Defendre, J., Pizzano, G.M., Dave, R.N., 2020. Exploring tablet design options for tailoring drug release and dose via fused deposition modeling (FDM) 3D printing. Int. J. Pharm. 591, 119987.
Han, X., Ghoroi, C., Dave, R., 2013a. Dry coating of micronized API powders for improved dissolution of directly compacted tablets with high drug loading. Int. J. Pharm. 442 (1–2), 74–85.
Han, X., Jallo, L., To, D., Ghoroi, C., Dave, R., 2013b. Passivation of high-surface-energy sites of milled ibuprofen crystals via dry coating for reduced cohesion and improved flowability. J. Pharm. Sci. 102 (7), 2282–2296.
Hancock, B.C., Carlson, G.T., Ladipo, D.D., Langdon, B.A., Mullarney, M.P., 2002. Comparison of the mechanical properties of the crystalline and amorphous forms of a drug substance. Int. J. Pharm. 241 (1), 73–85.
Hancock, B.C., Zografi, G., 1997. Characteristics and significance of the amorphous state in pharmaceutical systems. J. Pharm. Sci. 86 (1), 1–12.
Huang, S., Williams 3rd, R.O., 2018. Effects of the Preparation Process on the Properties of Amorphous Solid Dispersions. AAPS PharmSciTech 19 (5), 1971–1984.
Huang, Z., Xiong, W., Kunnath, K., Bhaumik, S., Dave, R.N., 2017. Improving blend content uniformity via dry particle coating of micronized drug powders. Eur. J. Pharm. Sci. 104, 344–355.
Israelachvili, J., 1992. Intermolecular and Surfaces Forces, 2nd edn. Academic Press, New York.
Iyer, R., Hegde, S., Zhang, Y.E., Dinunzio, J., Singhal, D., Malick, A., Amidon, G., 2013. The impact of hot melt extrusion and spray drying on mechanical properties and tableting indices of materials used in pharmaceutical development. J. Pharm. Sci. 102 (10), 3604–3613.
Iyer, R., Petrovska Jovanovska, V., Berginc, K., Jaklic, M., Fabiani, F., Harlacher, C., Huzjak, T., Sanchez-Felix, M.V., 2021. Amorphous Solid Dispersions (ASDs): The Influence of Material Properties, Manufacturing Processes and Analytical Technologies in Drug Product Development. Pharmaceutics 13 (10).
Jallo, L.J., Dave, R.N., 2015. Explaining electrostatic charging and flow of surface-modified acetaminophen powders as a function of relative humidity through surface energetics. J. Pharm. Sci. 104 (7), 2225–2232.
Jallo, L.J., Chen, Y., Bowen, J., Etzler, F., Dave, R., 2012a. Prediction of Inter-particle Adhesion Force from Surface Energy and Surface Roughness. J. Adhes. Sci. Technol. 25 (4–5), 367–384.

Jallo, L.J., Ghoroi, C., Gurumurthy, L., Patel, U., Dave, R.N., 2012b. Improvement of flow and bulk density of pharmaceutical powders using surface modification. Int. J. Pharm. 423 (2), 213–225.
Johno, Y., Satomi, M., Nakashima, K., Shigematsu, T., Ono, B., 2009. Numerical simulation of particle settling and cohesion in liquid. J. Phys. Conf. Ser. 147.
Khougaz, K., Clas, S.D., 2000. Crystallization inhibition in solid dispersions of MK-0591 and poly(vinylpyrrolidone) polymers. J. Pharm. Sci. 89 (10), 1325–1334.
Kim, S., Bilgili, E., Dave, R.N., 2021. Impact of altered hydrophobicity and reduced agglomeration on dissolution of micronized poorly water-soluble drug powders after dry coating. Int. J. Pharm. 606, 120853.
Kim, S.S., Castillo, C., Sayedahmed, M., Dave, R.N., 2022. Reduced Fine API Agglomeration After Dry Coating for Enhanced Blend Uniformity and Processability of Low Drug Loaded Blends. Pharm. Res. 39 (12), 3155–3174.
Kim, S.S., Castillo, C., Cheikhali, M., Darweesh, H., Kossor, C., Dave, R.N., 2023. Enhanced blend uniformity and flowability of low drug loaded fine API blends via dry coating: The effect of mixing time and excipient size. Int. J. Pharm. 635, 122722.
Kunnath, K., Huang, Z., Chen, L., Zheng, K., Dave, R., 2018. Improved properties of fine active pharmaceutical ingredient powder blends and tablets at high drug loading via dry particle coating. Int. J. Pharm. 543 (1–2), 288–299.
Kunnath, K., Chen, L., Zheng, K., Davé, R.N., 2021. Assessing predictability of packing porosity and bulk density enhancements after dry coating of pharmaceutical powders. Powder Technol. 377, 709–722.
Kunnath, K.T., Tripathi, S., Kim, S.S., Chen, L., Zheng, K., Dave, R.N., 2023. Selection of Silica Type and Amount for Flowability Enhancements via Dry Coating: Contact Mechanics Based Predictive Approach. Pharm. Res. 40 (12), 2917–2933.
Leane, M., K. Pitt, G. Reynolds and G. Manufacturing Classification System Working (2015). "A proposal for a drug product Manufacturing Classification System (MCS) for oral solid dosage forms." Pharm Dev Technol **20**(1): 12-21.
Li, Y., Yu, J., Hu, S., Chen, Z., Sacchetti, M., Sun, C.C., Yu, L., 2019. Polymer Nanocoating of Amorphous Drugs for Improving Stability, Dissolution, Powder Flow, and Tabletability: The Case of Chitosan-Coated Indomethacin. Mol. Pharm. 16 (3), 1305–1311.
Li, J., Zhao, J., Tao, L., Wang, J., Waknis, V., Pan, D., Hubert, M., Raghavan, K., Patel, J., 2015. The effect of polymeric excipients on the physical properties and performance of amorphous dispersions: Part I, free volume and glass transition. Pharm. Res. 32 (2), 500–515.
Lin, Z., Cabello, B., Kossor, C., Dave, R., 2024. Facilitating direct compaction tableting of fine cohesive APIs using dry coated fine excipients: Effect of the excipient size and amount of coated silica. Int. J. Pharm. 660, 124359.
Liversidge, G.G., Cundy, K.C., 1995. Particle size reduction for improvement of oral bioavailability of hydrophobic drugs: I. Absolute oral bioavailability of nanocrystalline danazol in beagle dogs. Int. J. Pharm. 125 (1), 91–97.
Lu, J., Obara, S., Ioannidis, N., Suwardie, J., Gogos, C., Kikuchi, S., 2016. Understanding the Processing Window of Hypromellose Acetate Succinate for Hot-Melt Extrusion, Part I: Polymer Characterization and Hot-Melt Extrusion. Adv. Polym. Tech. 37 (1), 154–166.
Marsac, P.J., Shamblin, S.L., Taylor, L.S., 2006. Theoretical and practical approaches for prediction of drug-polymer miscibility and solubility. Pharm. Res. 23 (10), 2417–2426.
Massimilla, L., Donsì, G., 1976. Cohesive forces between particles of fluid-bed catalysts. Powder Technol. 15 (2), 253–260.
Mendonsa, N., Almutairy, B., Kallakunta, V.R., Sarabu, S., Thipsay, P., Bandari, S., Repka, M.A., 2020. "Manufacturing strategies to develop amorphous solid dispersions: An overview." J Drug Deliv. Sci. Technol. 55.
Monschke, M., Kayser, K., Wagner, K.G., 2021. Influence of Particle Size and Drug Load on Amorphous Solid Dispersions Containing pH-Dependent Soluble Polymers and the Weak Base Ketoconazole. AAPS PharmSciTech 22 (1), 44.
Mooter, G.V., 2011. The use of amorphous solid dispersions: A formulation strategy to overcome poor solubility and dissolution rate. Drug Discov. Today Technol. 9 (2), e71–e174.
Moseson, D.E., Parker, A.S., Beaudoin, S.P., Taylor, L.S., 2020. Amorphous solid dispersions containing residual crystallinity: Influence of seed properties and polymer adsorption on dissolution performance. Eur. J. Pharm. Sci. 146, 105276.
Mullarney, M.P., Beach, L.E., Davé, R.N., Langdon, B.A., Polizzi, M., Blackwood, D.O., 2011. Applying dry powder coatings to pharmaceutical powders using a comil for improving powder flow and bulk density. Powder Technol. 212 (3), 397–402.
Nase, S.T., Vargas, W.L., Abatan, A.A., McCarthy, J.J., 2001. Discrete characterization tools for cohesive granular material. Powder Technol. 116 (2–3), 214–223.
Newman, A., Knipp, G., Zografi, G., 2012. Assessing the performance of amorphous solid dispersions. J. Pharm. Sci. 101 (4), 1355–1377.
Nokhodchi, A., Maghsoodi, M., Hassan-Zadeh, D., Barzegar-Jalali, M., 2007. Preparation of agglomerated crystals for improving flowability and compactibility of poorly flowable and compactible drugs and excipients. Powder Technol. 175 (2), 73–81.
Prescott, J.K., Garcia, T.P., 2001. A solid dosage and blend content uniformity troubleshooting diagram. Pharm. Technol. 25 (3), 68.
Rahman, M., Coelho, A., Tarabokija, J., Ahmad, S., Radgman, K., Bilgili, E., 2020. Synergistic and antagonistic effects of various amphiphilic polymer combinations in enhancing griseofulvin release from ternary amorphous solid dispersions. Eur. J. Pharm. Sci. 150, 105354.
Rumondor, A.C., Ivanisevic, I., Bates, S., Alonzo, D.E., Taylor, L.S., 2009a. Evaluation of drug-polymer miscibility in amorphous solid dispersion systems. Pharm. Res. 26 (11), 2523–2534.
Rumondor, A.C., Marsac, P.J., Stanford, L.A., Taylor, L.S., 2009b. Phase behavior of poly (vinylpyrrolidone) containing amorphous solid dispersions in the presence of moisture. Mol. Pharm. 6 (5), 1492–1505.
Sarode, A.L., Sandhu, H., Shah, N., Malick, W., Zia, H., 2013. Hot melt extrusion (HME) for amorphous solid dispersions: predictive tools for processing and impact of drug-polymer interactions on supersaturation. Eur. J. Pharm. Sci. 48 (3), 371–384.
Sarode, A.L., Malekar, S.A., Cote, C., Worthen, D.R., 2014. Hydroxypropyl cellulose stabilizes amorphous solid dispersions of the poorly water soluble drug felodipine. Carbohydr. Polym. 112, 512–519.
Schonfeld, B.V., Westedt, U., Wagner, K.G., 2021. Compression of amorphous solid dispersions prepared by hot-melt extrusion, spray drying and vacuum drum drying. Int J Pharm X 3, 100102.
Schulze, D., 2008. Powders and bulk solids : behavior, characterization, storage and flow. Springer, Berlin; New York.
Schulze, D., 2021. Powders and bulk solids. Springer.
Sekiguchi, K., Obi, N., Ueda, Y., 1964. Studies on Absorption of Eutectic Mixture. Ii. Absorption of Fused Conglomerates of Chloramphenicol and Urea in Rabbits. Chem Pharm Bull (tokyo) 12, 134–144.
Shi, L., Chattoraj, S., Sun, C.C., 2011. Reproducibility of flow properties of microcrystalline cellulose — Avicel PH102. Powder Technol. 212 (1), 253–257.
Sinka, I.C., Schneider, L.C., Cocks, A.C., 2004. Measurement of the flow properties of powders with special reference to die fill. Int. J. Pharm. 280 (1–2), 27–38.
Thalberg, K., Lindholm, D., Axelsson, A., 2004. Comparison of different flowability tests for powders for inhalation. Powder Technol. 146 (3), 206–213.
Tidau, M., Kwade, A., Finke, J.H., 2019. Influence of High, Disperse API Load on Properties along the Fused-Layer Modeling Process Chain of Solid Dosage Forms. Pharmaceutics 11 (4).
Venkatesh, G.M., Barnett, M.E., Owusu-Fordjour, C., Galop, M., 2001. Detection of low levels of the amorphous phase in crystalline pharmaceutical materials by thermally stimulated current spectrometry. Pharm. Res. 18 (1), 98–103.
Vrentas, J.S., Duda, J.L., Ling, H.C., 1988. Antiplasticization and volumetric behavior in glassy polymers. Macromolecules 21 (5), 1470–1475.
Xie, X., Puri, V.M., 2007. Uniformity of Powder Die Filling Using a Feed Shoe: A Review. Part. Sci. Technol. 24 (4), 411–426.
Yu, A.B., Feng, C.L., Zou, R.P., Yang, R.Y., 2003. On the relationship between porosity and interparticle forces. Powder Technol. 130 (1–3), 70–76.
Zheng, K., Lin, Z., Capece, M., Kunnath, K., Chen, L., Dave, R.N., 2019. Effect of Particle Size and Polymer Loading on Dissolution Behavior of Amorphous Griseofulvin Powder. J. Pharm. Sci. 108 (1), 234–242.